Manipulator Control System for Remote USG Examinantion

Submitted: 12th January 2019; accepted: 13th April 2019

Adam Kurnicki, Bartłomiej Stańczyk

DOI: 10.14313/JAMRIS/2-2019/18

Abstract:
The article presents a control algorithm of a robotic manipulator used as the main component of a system for a remote noninvasive medical ultrasound examination. This algorithm has been developed within the ReMeDi (Remote Medical Diagnostician) project. At the beginning of the article, the manipulator kinematics, its mechanical construction and the control system structure as a part of the telemanipulation system is shown. The essential components of the control system are discussed in detail. Then problems and solutions connected with the generation and conversion of the position and orientation of the reference signals are presented. Finally, the results of the evaluations with users are discussed.

Keywords: *remote medical examination, telemedicine, medical robot, manipulator, control system*

1. Introduction

The demographic development of modern societies, characterised by increase in the number of elderly people, drives up the demand for specialised medical care and for advanced diagnostic facilities. Unfortunately, primary healthcare centres and provincinal hospitals in most countries, especially developing ones, usually lack such facilities and do not always provide specialised services because of a lack of physicians. Shortage of qualified specialists often leads to misdiagnosis, which can cause further deterioration in patient's health, or even lead to demise. Such circumstances provide an incentive for the development of many types of telemedicine-related services, ranging from telerehabilitation [22], teledentistry [10], etc. to telesurgery [28]. Medical robots are successfully employed in numerous telemedicine systems. The most technologically advanced and best known are surgical robots [19, 30].

Successful medical treatment normally depends on a timely and correct diagnosis which is crucial in typical emergency situations. A medical specialist needs some time to get to a patient from home or another hospital. If a doctor could perform diagnosis remotely and make a decision about surgical intervention, the hospital staff could use the time during which the doctor is travelling and prepare the patient. In order to help in such situations, a number of telerobotic systems were developed. Currently researchers work on newer, more advanced and universal solutions. Some of them reached the level of commercial products, e.g. *VGO* [4] used for medical teleconsultation, *MEDIROB* [2] for echocardiography examination and *MELODY* [1] for abdominal ultrasonography. To the best knowledge of the authors, there are currently no devices allowing a complete remote medical examination (i.e. interview, auscultation, palpation and USG examinations) and diagnosis based on contemporary medical standards, apart from the ReMeDi [3] system.

The Remote Medical Dignostician (ReMeDi) is a multifunctional robotic system which allows to perform a real remote physical and ultrasonographic (USG) examination [6, 21, 27]. The first version of this system was designed and made during the ReMeDi project [3] funded by the European Union's Research and Innovation 7th Framework Programme (EU FP7). Nowadays system is developed within project: "Research and innovation" activity 1.2 RPO WL 2014-2020 funded by Lublin Enterprise Support Agency.

The ReMeDi system is a typical teleoperation system, which basic principle of work is illustrated in Fig. 1. It can be seen as two subsystems, physically spaced apart. The first one, called ReMeDi Robot, is located on the patient's site (in a provincinal hospital or medical centre) and the second, called DiagUI (Diagnostician User Interface), is on the doctor's site (in another hospital or doctor's home). The doctor plays the role of operator and the system enables him to carry out remote medical examination of the patient in the way that is essentially similar to the traditional examination. During the examination doctor moves and rotates a dummy USG probe held in the palm. The dummy probe constitutes the top part of a haptic interface (see left part of Fig. 1). It allows to generate and send position and orientation demands for the real USG probe, which examines the patient. In order to obtain the right ultrasound image, doctor has to properly position the real probe on the patient body. This is possible, because the real probe is the end effector of the manipulator fixed to the mobile ReMeDi robot (see right part of Fig. 1) and follows the required movements. At the same time, the forces acting on the ultrasound probe should be conveyed to the dummy probe via the haptic interface so that the doctor can feel the stiffness and the geometry of the patient's body. The use of a fairly advanced vision system allows the doctor to observe the patient's body and the real probe online. The medical interview with the patient is performed by the doctor due to the integration of the teleconferencing system on both sites of the ReMeDi system. All measurement, control and audio-video signals are transmitted via the Internet.

Ultrasound examination is one of the most fre-

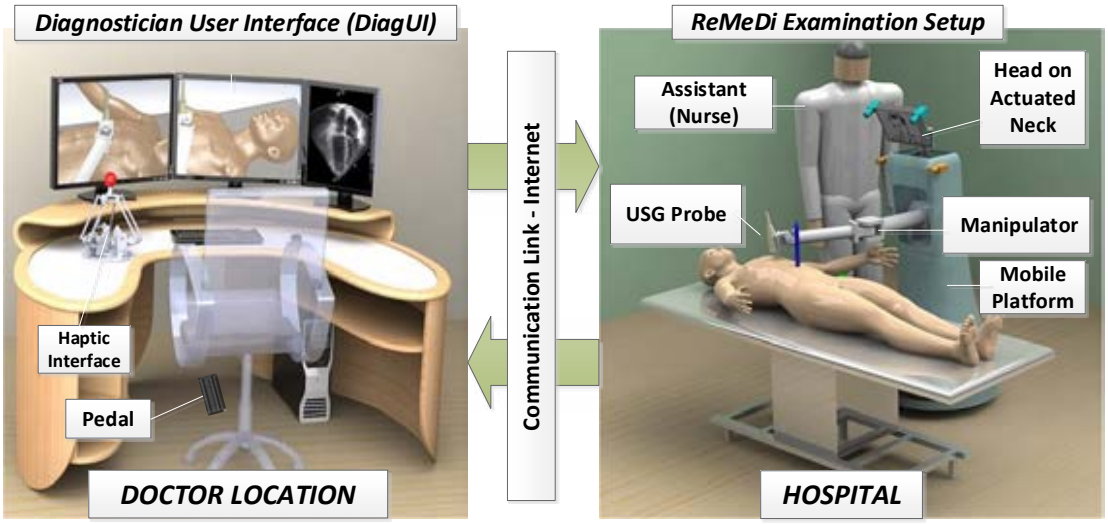

Fig. 1. ReMeDi system overview

quently used diagnostics methods, as well as it provides the most specialist diagnostic information during medical emergencies. From the teleoperation point of view it is the most complex and complicated part of a remote medical examination. The key in the implementation and realisation of this examination is the use of a robot with a manipulator. The robotic solutions for tele-echography proposed in the literature can be divided into two groups. The first group [1, 5, 9, 13] addresses relativelly small and portable manipulators, usually intended for dedicated type of the USG examination. They allow the doctor to perform only small transitions and rotation of the USG probe in the region where assistant placed and held them. In the second group [11, 12, 16, 18, 24], independent robots are equipped with manipulators (usually anthropomorphic) which allows the physician to perform full control of the probe position and orientation. The ReMeDi arm mechanics and control system were designed to give the physician the operational ability addressed by the second group. Due to the fact that it performs manipulations in a direct contact with the patient's body, it should be safe, which is facilitated by reliability, stability, low stiffness and low mass of the manipulator. Unfortunately, the requirements of the user (physician) are slightly different. He would like the required position and orientation of the probe to be accurately reproduced (without inertia and drift). In addition, he would like to be able to feel the touch and rigidity of the patient's body as much as possible (high stiffness of the manipulator is required). In this connection, while designing the ReMeDi robot and its control system, compromise solutions were used, which took into account the above mentioned issues.

There is a quite wide variety of control system architectures dedicated for manipulators used in tele-echography research. Most of them is based on classical manipulator control architecture with inner position [17] or velocity [16, 31] control loop (usually with PID controller) at joint level. Joint references are computed in outer loop, which performs Cartesian control through velocity based (less often position based) inverse kinematics. Mathiassen *et al.* [16] propose to control the manipulator implementing a compliance force control algorithm before velocity based inverse kinematics. The robotic tele-echography system developed by Koizumi *et al.* [12] uses impedance control at Cartesian position control level. While the orientation is controlled directly with the use of continuous path controller [11]. More advanced and complicated control architecture dedicated for robotic-assisted tele-echography manipulator was developed by Luıs Santos and Rui Cortesao. In [23] they applied indirect force control (admittance control) for Cartesian motion control loop to establish the contact dynamics between the echographic probe and the patient. The orientation is controlled without the admitance control loop. Additionally, the motion controller has a velocity model-reference adaptive control (AOB) in the joint space level, driven by task space posture errors. A two-task hierarchy architecture with posture optimization is proposed in [24], where Cartesian force control is the primary task, orientation control is the secondary task, and posture optimization is performed in the null space of all prioritized tasks.

This paper focuses on the challenges related to the design of the control system of the ReMeDi manipulator which allows a doctor to carry out remote medical examination, including auscultation and different modes of an ultrasonographic examination. In section 2 a general overview of ReMeDi telemanipulation system is presented. This section outlines the construction and kinematics of the manipulator as the most important parts of the telemanipulation system. In section 3 the manipulator control system structure and its components are discussed in detail. Algorithms that generate position and orientation reference signals based on the received demands from the Master side are shown in section 4. Finally, some results of users evaluation are discussed in section 5.

2. ReMeDi Teleoperation System

The ReMeDi system employs bilateral teleoperation architecture, which general scheme is shown in Fig. 2. It has a classical structure [14, 20] with such components as: Doctor, Master, Communication channel, Slave and Environment – mainly the Patient's body.

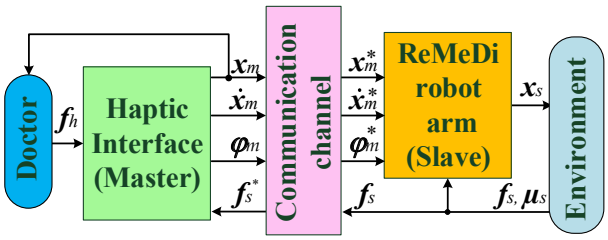

Fig. 2. Structure of the ReMeDi bilateral teleoperation system

The main system components: Master – the haptic interface and Slave – the ReMeDi robot manipulator are presented in Fig 3. Since these components are separated in their location, they have to exchange information (i.e. actual master input device: position $\boldsymbol{x}_m \in \mathbb{R}^3$, velocity $\dot{\boldsymbol{x}}_m \in \mathbb{R}^3$, orientation angles $\boldsymbol{\varphi}_m \in \mathbb{R}^3$ and forces $\boldsymbol{f}_s \in \mathbb{R}^3$ measured on the slave side) in real time, over the Communication channel (Internet) at quite considerable distances. The system features such undesired phenomenon as variable communication latencies, which are discussed in [7, 14]. In order to cope with this issue, the communication channel was equipped with wave variable algorithms. This solution is described in more detail in [14]. The transmitted signals $\boldsymbol{f}_s$, $\boldsymbol{x}_m$, $\dot{\boldsymbol{x}}_m$ and $\boldsymbol{\varphi}_m$ can be disturbed in the communication channel and therefore they are represented by the following symbols: $\boldsymbol{f}_s^*$, $\boldsymbol{x}_m^*$, $\dot{\boldsymbol{x}}_m^*$ and $\boldsymbol{\varphi}_m^* \in \mathbb{R}^3$ on the opposite side.

2.1. Master – Haptic Interface

The haptic interface (see Fig. 3a) is the core of the Master component. It consists of a pure 3D translational manipulator built as a motorised parallel robot with delta type kinematics [8]. It is used as a translation input device. A passive 3 DoF mechanism is mounted with a dummy USG probe at the top of the delta robot. Its range of motion corresponds to the hand movement pivoting at the wrist and plays the role of an orientation input device.

The haptic interface is controlled by the force controller, designed and deployed by PERCRO Lab [29]. The force controller computes the values of torques for each actuated joint of the delta robot as the sum of: the torques corresponding to the gravity and friction compensation of the haptic interface and the torques corresponding to force $\boldsymbol{f}_s$, which is acting on the real probe as a reaction to patient's body touch. It is a realisation of the force feedback and allows to produce true-to-life touch sensations on the doctor's hand. As an effect of exertion of force $\boldsymbol{f}_h \in \mathbb{R}^3$ by the doctor to the translation input device, the dummy probe moves

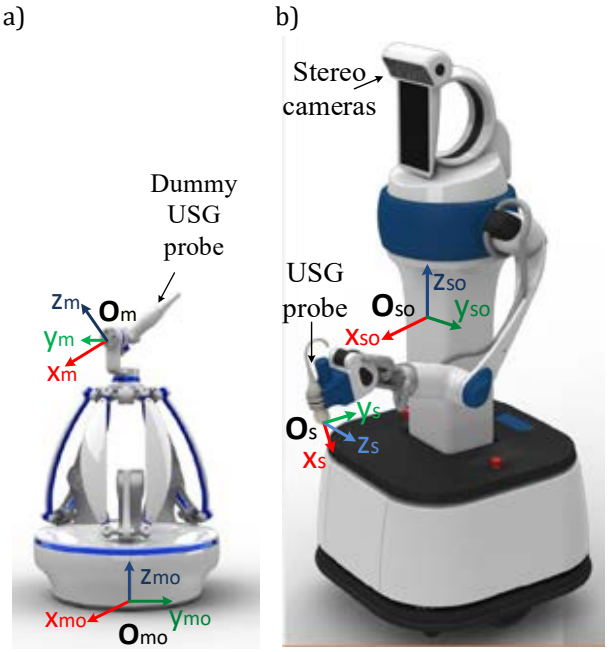

Fig. 3. ReMeDi teleoperation system components a – haptic interface, b – ReMeDi robot with manipulator

over distance represented by the change of position signal $\boldsymbol{x}_m$. The actual values of the signal $\boldsymbol{x}_m$ are calculated according to rules described in [8] based on the values of the delta robot joints angles, measured by encoders. They are used as reference values for the position control of the real probe.

The values of the joint angles $\boldsymbol{\varphi}_m$ read from encoders mounted on each joint of the orientation input device are used as reference values for control of the orientation of the ultrasound probe.

All of the measured vectors of Cartesian positions $\boldsymbol{x}_m$, velocities $\dot{\boldsymbol{x}}_m$ and Euler angles $\boldsymbol{\varphi}_m$ of the tip of the dummy probe are expressed in the master base coordination frame $\mathcal{O}_{mo} - x_{mo}y_{mo}z_{mo}$, shown in Fig. 3a.

2.2. Slave – ReMeDi Manipulator

The Slave component is based on a 7DoF human-sized manipulator mounted on the left side of the ReMeDi robot (see Fig. 3b). Several requirements were stated for the development of the ReMeDi arm in [15, 21, 27]. From the kinematics point of view, the most important is, that the arm should allow to perform all the typical echocardigraphy and abdominal USG examinations. To achieve this goal, the manipulator placed on the patient's site has to reveal similar physical characteristics to the human arm, so that the doctor can drive it as he would move his own arm during medical examination. According to [26], analysis of human arms reveals, that the minimum number of DOFs used for their reproduction is 7. The resulting design of the ReMeDi manipulator, shown in Fig. 4a, was performed by the ACCREA Engineering company.

The manipulator consists of: two rotational joints, first at the torso (turntable) and second at the elbow, two spherical joints with 2 DoFs at the shoulder and the wrist, and one additional, rotational joint at the probe (end-effector). The Denavit-Hartenberg para-

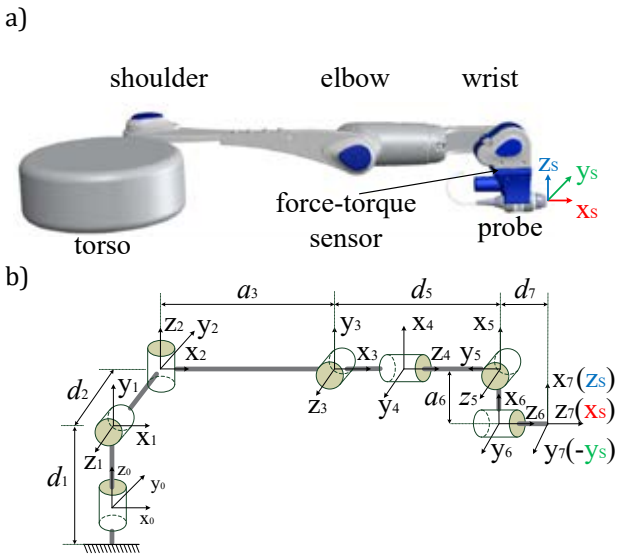

Fig. 4. ReMeDi 7 DoF manipulator
a – physical construction, b – kinematics structure and link coordinate systems

meters for the manipulator are listed in Table 1, the corresponding set of frames is shown in Fig. 4b.

Tab. 1. Manipulator Denavit-Hartenberg parameters

Joint no	Link offset a_i [m]	Link twist α_i [rad]	Link length d_i [m]	Joint angle q_i [rad]
1	0.0	$\pi/2$	0.35	q_1
2	0.0	$-\pi/2$	-0.26	q_2
3	0.4	$\pi/2$	0.0	q_3
4	0.0	$\pi/2$	0.0	$q_4 + \pi/2$
5	0.0	$-\pi/2$	0.32	q_5
6	-0.115	$\pi/2$	0.0	q_6
7	0.0	0.0	0.03	q_7

The ReMeDi arm is redundant and reaches 1m in length. Its kinematic structure is optimal in the sense of size/workspace relation so that the probe is capable of reproducing every doctor's movement performed during all the required USG examinations.

Relative to the patient's body, the manipulator is rigid. It is built with the use of aluminium/steel construction elements and typical electro-mechanical components like: DC motors with harmonic gears and incremental encoders mounted on the shaft. The maximal contact force, which could be generated at the probe tip is 40 N.

The hardware layer of the ReMeDi arm control system is based on a PC computer with a real-time operating system and a specialised, digital unit, called JointsController, manufactured by the ACCREA Engineering. Thus the deployment of the control system (arm control algorithms) is distributed between the two already mentioned hardware components. In general, this control system realises position control strategy. The ReMeDi arm control strategy and its particular control system components are presented in details in section 3.

In order to provide force feedback to the haptic interface, the arm is equipped with a dedicated custom built six-axis force/torque sensor (fts) mounted in series betweeen the last joint of the arm and the probe mounting mechanism.

The end-effector pose $\boldsymbol{\xi}_s$ (i.e. Cartesian position $\boldsymbol{x}_s \in \mathbb{R}^3$ and orientation matrix $\boldsymbol{R}_s \in \mathbb{R}^{3x3}$) and measured by fts and transformed to the tip of the real probe (see Fig. 4a): forces $\boldsymbol{f}_s$ and torques $\boldsymbol{\mu}_s$ are expressed in the slave base coordination frame $\mathcal{O}_{so} - x_{so}y_{so}z_{so}$, shown in Fig. 3b.

3. Manipulator Control System

The architecture of the ReMeDi arm control system is an evalution of the previous work [26]. The general block diagram of this architecture is presented in Fig. 5. From the point of view of the position and orientation control strategy, it has a cascaded structure, composed of two parts. The internal loop, formed by the two blocks: *ReMeDi Arm* and *Position Controller* is used to control the position and orientation of the arm in joint space, i.e. it tracks the reference trajectory $\boldsymbol{q}_{sd} \in \mathbb{R}^7$ by the vector of the actual joint position values $\boldsymbol{q}_s \in \mathbb{R}^7$. The external loop serves the realisation of the control algorithms in the task space. This part consists of the *Demanded Velocity Vector Calculation and Admittance Control*, an integrator and *IK-Inverse Kinematics* blocks. The *FK - Forward Kinematics* block is used to calculate the actual $\boldsymbol{\xi}_s$ and demanded $\boldsymbol{\xi}_{sd}$ end-effector pose based on the measured $\boldsymbol{q}_s$ and desired $\boldsymbol{q}_{sd}$ position values of the arm joints. There is one additional, very important block, which manages the ReMeDi arm controller - *Arm Control System Manager*. The main part of the *Position Controller* was physically implemented in JointsController (see Fig. 6). The algorithms, which realise the functionalities of all other blocks are executed under the real-time system of a PC based controller.

The communication between the PC and JointsController is realised through an ethernet connection with UDP protocol.

3.1. Position Controller

The *Position Controller* implements seven independent joint position control systems. Each of these systems has a form of position-velocity-torque cascade control structure, presented in Fig. 7. Every control loop, shown there, is a PID-based control algorithm, that causes the tracking of the demanded position value q_{isd} by the actual position value q_{is} of *i*-th joint.

The torque control loop is performed by DC motor servo controllers (current controllers - parts of DC Drives). The velocity and position control loops are implemented in the main motion controller (MMC) - part of JointsController (see hardware architecture shown in Fig. 6). JointsController is a hierarchical, multichip controller, which supports all seven DC drives, i.e. counts impulses from incremental encoders by the quadrature encoders (encoder interfaces built on the basis of seven STM32F1 microcontrollers) and

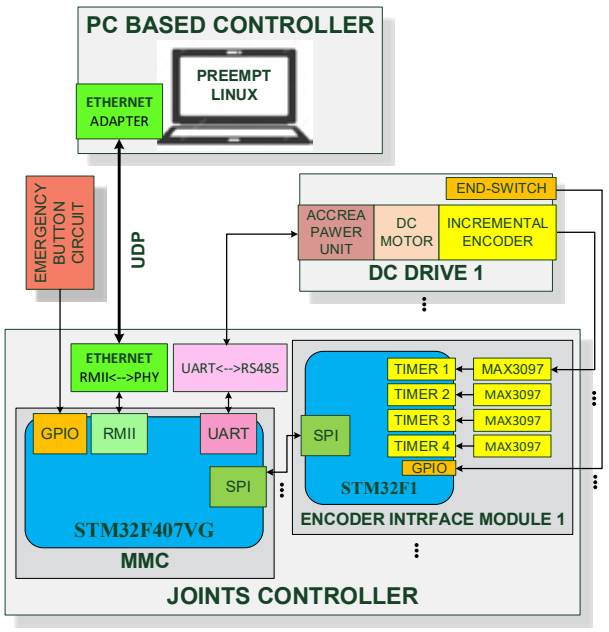

Fig. 6. Simplified hardware architecture of the ReMeDi arm control system

sends demands to current controller from the MMC via an RS485 interface. The MMC is a microcontroller STM32F407VG loaded with a program, which performs four basic tasks:

- communication with the higher-level controller (PC based controller) through the Ethernet,
- communication with DC drive power units through UART,
- acquisition of data from encoder interface modules through SPI ,
- execution (with 1 kHz) of the above-mentioned position-velocity control loops together with gravity and static friction compensation algorithms.

The gravity compensation algorithm results in correction of the torque signal τ_{isc} by torque τ_{isg} (see Fig. 7) obtained from the gravity model of the manipulator. Since harmonic gears are parts of the manipulator drives, the control quality is significantly impacted by their static friction. In order to eliminate this issue, a static friction compensation algorithm was used. This algorithm is based on the principle of a relay with hysteresis. The sign of the compensation torque τ_{isf} depends on the sign of the demanded velocity signal for the velocity control loop. The change of the τ_{isf} signal sign is not affected by the change of the demanded velocity value if the demanded velocity value is less than the arbitrarily chosen velocity threshold. The value of τ_{isf} equals the experimentally identified value of the drive static friction.

3.2. Inverse Kinematics

The values of the desired joint positions $\boldsymbol{q}_{sd}$ for the position control loop (see Fig. 5) result from the integration of the reference joint velocities $\dot{\boldsymbol{q}}_{sd} \in \mathbb{R}^7$. The velocity vector $\dot{\boldsymbol{q}}_{sd}$ is calculated by the *I*nverse *K*inematics block from the arm end-effector desired velocity vector $\dot{\boldsymbol{X}}_{sd} \in \mathbb{R}^6$. The vector $\dot{\boldsymbol{X}}_{sd} = [\dot{\boldsymbol{x}}_{sd}, \boldsymbol{\omega}_{sd}]$ consists of two vectors: the desired linear $\dot{\boldsymbol{x}}_{sd} \in \mathbb{R}^3$ and desired angular $\boldsymbol{\omega}_{sd} \in \mathbb{R}^3$ velocities, expressed with respect to the base frame $\mathcal{O}_{so} - x_{so}y_{so}z_{so}$ presented in Fig. 3b.

Since the manipulator forms a redundant kinematic chain, to solve the inverse kinematics problem a pseudoinverse control algorithm [26] is used:

$$\dot{\boldsymbol{q}}_{sd} = \boldsymbol{J}_s^{\#}\dot{\boldsymbol{X}}_{sd} + [\boldsymbol{I} - \boldsymbol{J}_s^{\#}\boldsymbol{J}_s]\dot{\boldsymbol{q}}_{sd0}, \tag{1}$$

where: $\boldsymbol{J}_s^{\#}$ is a Moore–Penrose pseudoinverse of the arm Jacobian $\boldsymbol{J}_s \in \mathbb{R}^{6x7}$, $\dot{\boldsymbol{q}}_{sd0} \in \mathbb{R}^7$ is an arbitrary value of the joint velocity vector.

3.3. Demanded Velocity Vector Calculation and Admittance Control

In order to improve the contact stability and to avoid large contact forces, the arm should be compliant. Since the arm is designed as a mechanically stiff structure, it is necessary to apply a compliant control algorithm - admittance control. The implemented admittance control algorithm is based on the force-torque $\boldsymbol{h}_s = [\boldsymbol{f}_s, \boldsymbol{\mu}_s] \in \mathbb{R}^6$ measurement recalculated to the end-effector tip. Regarding the algorithm presented in [23] and [24] not only the translational mo-

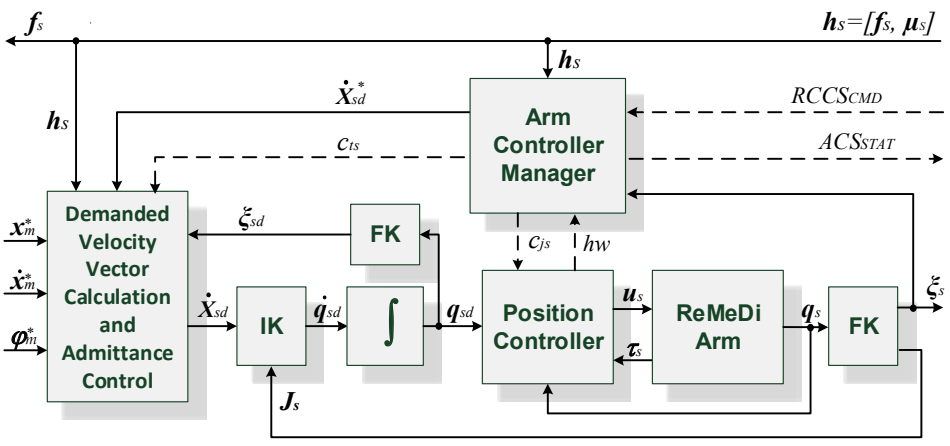

Fig. 5. ReMeDi arm control system architecture

tion is modified by admittance controller but the rotational (orientation) as well. The desired position or the velocity vector is corrected by its displacement or velocity respectively, calculated from the impedance equations [26] for translational and rotational motion:

$$\boldsymbol{f}_s = M\ddot{\boldsymbol{x}}_{dc} + D\dot{\boldsymbol{x}}_{dc} + K\boldsymbol{x}_{dc}, \tag{2}$$

$$\boldsymbol{\mu}_s = M_o\dot{\boldsymbol{\omega}}_{dc} + D_o\boldsymbol{\omega}_{dc} + K_o\boldsymbol{\varepsilon}_{dc}, \tag{3}$$

where: $\ddot{\boldsymbol{x}}_{dc}, \dot{\boldsymbol{x}}_{dc}, \boldsymbol{x}_{dc} \in \mathbb{R}^3$ are translational acceleration, velocity and displacement, $\dot{\boldsymbol{\omega}}_{dc}, \boldsymbol{\omega}_{dc}, \boldsymbol{\varepsilon}_{dc} \in \mathbb{R}^3$ are angular acceleration, velocity and displacement, M, M_o, D, D_o, K, K_o are inertia, damping and stiffness positive scalar parameters chosen experimentally (M=4 kg, D=63 Ns/m, K=500 N/m, M_o=0.04 kgm^2, D_o=1.3 Nms/rad, K_o=10 Nm/rad). This algorithm establishes a virtual mass-spring-damper system on the end-effector so that the arm becomes compliant.

Together with the admittance control, a 2nd order low-pass filters for translational and rotational motion:

$$\frac{1}{(2\pi f_c)^2}\ddot{\boldsymbol{x}}_{sdf} + \frac{1}{\pi f_c}\dot{\boldsymbol{x}}_{sdf} + \boldsymbol{x}_{sdf} = \boldsymbol{x}_d, \tag{4}$$

$$\frac{1}{(2\pi f_{co})^2}\dot{\boldsymbol{\omega}}_{sdf} + \frac{1}{\pi f_{co}}\boldsymbol{\omega}_{sdf} + \boldsymbol{\varepsilon}_{sdf} = \boldsymbol{\varepsilon}_d, \tag{5}$$

were implemented. Filters with cut-off frequencies f_c and f_{co} protect the arm against rapid changes of the desired position $\boldsymbol{x}_d \in \mathbb{R}^3$ and orientation angles $\boldsymbol{\varepsilon}_d \in \mathbb{R}^3$ commanded by the master device.

Finally, the desired position $\boldsymbol{x}_{sd} \in \mathbb{R}^3$ and orientation angles $\boldsymbol{\varepsilon}_{sd} \in \mathbb{R}^3$ are given as:

$$\boldsymbol{x}_{sd} = \boldsymbol{x}_{sdf} + \boldsymbol{x}_{dc}, \tag{6}$$

$$\boldsymbol{\varepsilon}_{sd} = \boldsymbol{\varepsilon}_{sdf} + \boldsymbol{\varepsilon}_{dc}. \tag{7}$$

Taking into account the equations (2) - (7) and assuming that: $1/(2\pi f_c)^2 = M/K$, $1/\pi f_c = D/K$, $1/(2\pi f_{co})^2 = M_o/K_o$ and $1/\pi f_{co} = D_o/K_o$ the desired velocity vector $\dot{\boldsymbol{X}}_{sd}$ used by the inverse kinematics algorithm (1) can be calculated from the following equations:

$$M\ddot{\boldsymbol{x}}_{sd} + D\dot{\boldsymbol{x}}_{sd} = \boldsymbol{f}_s + K(\boldsymbol{x}_d - \boldsymbol{x}_{sd}), \tag{8}$$

$$M_o\dot{\boldsymbol{\omega}}_{sd} + D_o\boldsymbol{\omega}_{sd} = \boldsymbol{\mu}_s + K_o(\boldsymbol{\varepsilon}_d - \boldsymbol{\varepsilon}_{sd}). \tag{9}$$

The desired pose $\boldsymbol{\xi}_{sd} = [\boldsymbol{x}_{sd}, \boldsymbol{\varepsilon}_{sd}]$ (see Fig. 5) is calculated by forward kinematics from desired joint positions $\boldsymbol{q}_{sd}$. The desired orientation angles $\boldsymbol{\varepsilon}_d$ and $\boldsymbol{\varepsilon}_{sd}$ are represented in the implementation of the control algorithm by quaternions obtained by means of transformations described in [26].

The reference pose for slave $\boldsymbol{\xi}_d$ (i.e. the desired position $\boldsymbol{x}_d \in \mathbb{R}^3$ and the quaternion which represents the desired orientation matrix $\boldsymbol{R}_d \in \mathbb{R}^{3x3}$ or $\boldsymbol{\varepsilon}_d \in \mathbb{R}^3$ in equation (9)) is calculated based on the signals $\boldsymbol{x}^*_m$ and $\boldsymbol{\varphi}^*_m$ received from the haptic interface, according to the algorithms presented in section 4.

3.4. Arm Control System Manager

The *Arm Control System Manager* is composed of three functional elements: the arm decision maker (ADM), trajectory generators and the arm monitoring system. The arm monitoring system analyses the signals coming from the *Position Controller* (including the *hw* signal carrying information about the state of the hardware), which leads to the system failure detection and isolation (safety feature). On the basis of this information and control commands received from the ReMeDi Robot Central Control System ($RCCS_{CMD}$ - see more detailed information about RCCS in publication [25]) the ADM generates control commands: c_{ts} for task space control system part (i.e. for *Demand Velocity Vector Calculation block*) and c_{js} for joint space controller (i.e. *Position Controller*). The ADM also supervises trajectory generators. It switches sources (algorithms) of programmed arm movement trajectories (i.e. demanded velocity vector $\dot{\boldsymbol{X}}^*_{sd} \in \mathbb{R}^6$ values) according to RCCS commands and consequently to the ADM commands.

The Arm Decision Maker was designed in the form of a finite state machine, presented in Fig. 8. It operates on four main states: Startup, Active, Shutdown and Failure.

Just after Power is activated, the system goes directly to the Startup state, where low-level control components are initialised/run. When all the lower-level components have been run properly (i.e. signal *Startup_Done* has been set to "1") and the RCCS has initiated the startup procedure for the whole ReMeDi system (by setting $RCCS_{CMD}$ to the STARTUP value [25]) the system leaves the Startup state and goes to the Active state. In case an emergency button is pressed or any component indicates a failure state or the RCCS sends the FAILURE command (i.e. $RCCS_{CMD}$==FAILURE), the system goes into the Fai-

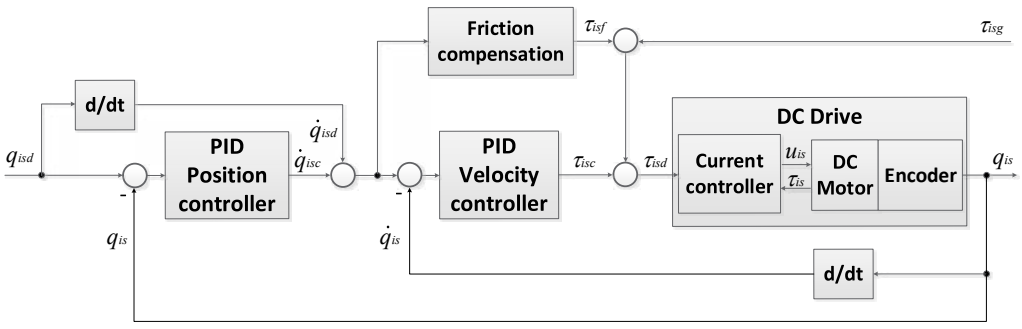

Fig. 7. Postion-Velocity-Torque cascade control structure – part of the position controller

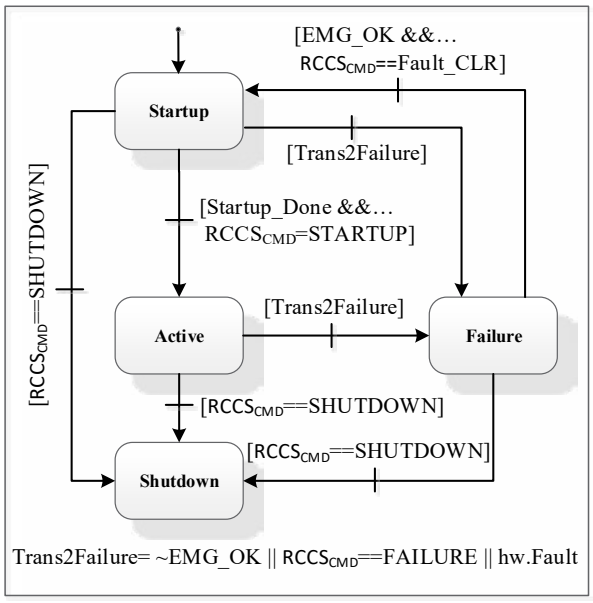

Fig. 8. Arm Decision Maker – finite state machine

lure state. Then the ADM sends information via a c_{js} signal to the *Position Controller* that it should run operations required in the failure state, i.e. disable drives, brake joints, etc. In order to switch off the ReMeDi arm in a controlled manner, the RCCS sends the SHUTDOWN command to the ADM, which starts the shutdown procedure. The high-level controller (RCCS) is informed about the current status of the arm control system by an *Arm Controller Manager* output signal ACS_{STAT} (see Fig. 5), which is in fact the output signal from the ADM and indicates its actual state.

The arm decision maker includes more elements than the four states presented in Fig. 8. Each of these states is represented by several substates. The most important and complex, from the medical examination point of view, is the Active state (see Fig. **??**). The Active state begins in one of four states:

- Homing - the procedure of initialisation/reset of arm joint encoders, executed when homing procedure has not yet been done (*Homing_DONE* is "0"),
- Wait for Arm Unsecure - the state preceding Homing, activated in case the arm hasn't been mechanically unlocked i.e. the sensor signal *ArmSecured* is "1",
- Rest Mode - the joint drives are disabled (relaxed in case there is no need to keep the arm power consumed), activated when homing has been already done and the arm is mechanically locked,
- GoTo Init Pose - the arm goes to the initial position in which the force-torque sensor is initialised and the arm is ready for preparation to the examination.

After the GoTo Init Pose procedure is completed, the algorithm goes to the Hold Pose state. This state indicates that all the moving parts of the arm should be stopped. It is the starting point for the other commonly used actions.

The Hand Lead and Tool Change states are used during arm preparation for examination. The former helps the assistant to manually position the arm close to the examined body part of the patient. In this case demanded arm pose is modified by an algorithm which maps measurements received from the force/torque sensor to demanded velocity vector $\dot{\boldsymbol{X}}^*_{sd}$. The Tool Change state allows the assistant to change the probe. When the Remote Examination state is active, the doctor remotely operates the arm. After the examination is finished and if the RCCS required parking procedure ($RCCS_{CMD}$== PARKING), the ADM goes to the Parking state. Trajectory generator leads the arm to the parking position. Finally, just after the arm has been secured (*ArmSecured* is set to "1"), the ADM activates the Rest Mode.

4. Determination of the Position and Orientation Setpoint

The manipulator control algorithm described in section 3 controls the position and orientation of the ultrasound probe in relation to the arm base coordinate system, which means that all of the variables associated with the control in the Cartesian space, are expressed relative to the base coordinate system of the slave manipulator $\mathcal{O}_{so} - x_{so}y_{so}z_{so}$ (see Fig. 3b). The signals coming from the master are expressed in the base coordinate system of the haptic interface $\mathcal{O}_{mo} - x_{mo}y_{mo}z_{mo}$ (see Fig. 3a). Therefore, all variables must be unified to a single coordinate system; in this case the slave coordinate system is chosen. Thus all calculations of the position and orientation setpoints are determined in the slave coordinate system. However, it is not necessary to perform a mathematical transformation of the master base coordinate system to the slave base coordinate system, since the default master X axis is perpendicular to the screen displaying the actual probe location to the doctor, and the X axis of the base slave system is parallel to the camera that generates this very image, so it is possible to assume that these coordinate systems are aligned and the transformation is replaced by the visual feedback.

In the implementation of the algorithm determining the position and orientation setpoints one should take into account a number of conditions related to the architecture and logical sequence of the ReMeDi system events and the requirements of the user (doctor), as described in [25]. Some of these conditions are the initial conditions for determining the position and orientation setpoints, which are determined at the moment of acquisition of the remote control of the manipulator by a doctor, i.e. the moment of pressing the pedal by the doctor (see Fig. 1) - the coupling of master and slave. Position and orientation setpoints are generally calculated as the sum of the increments of the position and orientation respectively (generated by the doctor on the haptic interface after the master and slave coupling) and the values of the position and orientation at the time of the coupling of the master and slave. This mechanism will be described in more detail in the subsequent sections.

With the orientation control, in order to ensure the comfort of the doctor (intuitive orientation change), it is also necessary to take into account the need for

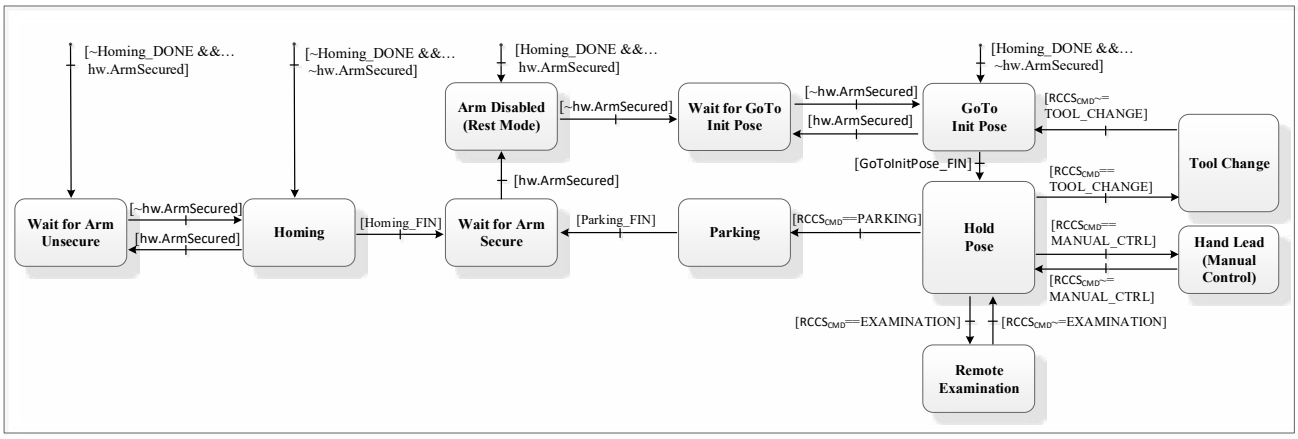

Fig. 9. Arm Decision Maker – Active state

proper synchronisation of coordinate systems of the manipulator tip $\mathcal{O}_s - x_s y_s z_s$ (see Fig. 3b) , and the coordinate system orientation of the orientation input device $\mathcal{O}_m - x_m y_m z_m$ (see Fig. 3a), ie. aligning of the probe dummy and the real probe before pressing the clutch pedal. This situation is shown by the diagram in Fig. 10, where the frames of the Master's probe $\mathcal{O}_{ml}$ and the Slave's probe $\mathcal{O}_{sl}$ are synchronised at the moment of system coupling. We developed three alternatives presented in the section 4.2, which were evaluated by the users during the system's evaluation.

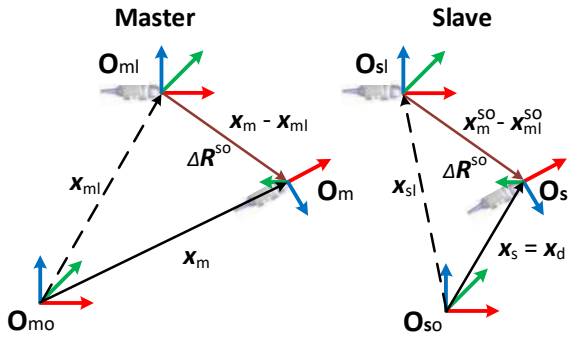

Fig. 10. Diagram showing the arrangement of the dummy and real probes at the moment of coupling and after a translation and rotation of the input device (axis colours: X – red, Y – green and Z – blue)

4.1. The Algorithm for Determining the Position Setpoints

The vector of the position setpoints $\boldsymbol{x}_d$ (see left side of Fig. 10) required as reference signal in the algorithm presented in section 3.3, in equation (8) is calculated using the following rule:

$$\boldsymbol{x}_d = \boldsymbol{x}_s = \boldsymbol{x}_{sl} + \boldsymbol{x}_m^{so} - \boldsymbol{x}_{ml}^{so}, \tag{10}$$

the right side of which is a sum of the manipulator end-effector position $\boldsymbol{x}_{sl} \in \mathbb{R}^3$, recorded at the time the coupling of the master and slave and the difference between the haptic interface positions: $\boldsymbol{x}_m^{so} \in \mathbb{R}^3$ - current and $\boldsymbol{x}_{ml}^{so} \in \mathbb{R}^3$ - registered at the moment of the coupling, which values are the values of the signal $\boldsymbol{x}_m^*$ (see Fig. 2 or Fig. 5) and are expressed relative to $\mathcal{O}_{so}$ - the base coordinate system of the manipulator.

4.2. The Algorithm for Determining the Orientation Setpoints

The mechanical structure of the orientation input device shown in Fig. 3a is such that the matrix of rotations $\boldsymbol{R}_m^{mo} \in \mathbb{R}^{3x3}$ is calculated based on the angle values measured on the consecutive Euler angle system:

$$\boldsymbol{R}_m^{mo} = \boldsymbol{R}_{z,\varphi mz}\boldsymbol{R}_{y,\varphi my}\boldsymbol{R}_{x,\varphi mx} = \boldsymbol{R}_m^{so}. \tag{11}$$

The doctor manipulating the orientation input device during the teleoperation, changes the orientation of the dummy probe according to the following equation:

$$\boldsymbol{R}_m^{so} = \Delta\boldsymbol{R}^{so}\boldsymbol{R}_{ml}^{so}, \tag{12}$$

where: $\boldsymbol{R}_m^{so}$, $\boldsymbol{R}_{ml}^{so} \in \mathbb{R}^{3x3}$ - current and registered at the time of coupling the master and slave matrices (11), expressed in the $\mathcal{O}_{so}$ coordinate system, $\Delta\boldsymbol{R}^{so} \in \mathbb{R}^{3x3}$ - the change (increment) of the orientation of the dummy probe expressed relative to the base $\mathcal{O}_{so}$ coordinate system. This operation is presented on left side diagram in Fig. 10. Rearranging the equation (12) we obtain:

$$\Delta\boldsymbol{R}^{so} = \boldsymbol{R}_m^{so}(\boldsymbol{R}_{ml}^{so})^{-1}, \tag{13}$$

Finally, the rotation matrix representing the orientation setpoint for the real ultrasound probe may be calculated according to the following formula:

$$\boldsymbol{R}_d = \boldsymbol{R}_s^{so} = \Delta\boldsymbol{R}^{so}\boldsymbol{R}_{sl}, \tag{14}$$

where: $\boldsymbol{R}_{sl} \in \mathbb{R}^{3x3}$ – the rotation matrix of the slave manipulator at the moment of the pressing of coupling pedal.

Depending on the number of axes of the coordinate systems defining the orientation of the dummy and the real ultrasound probe, which should be synchronised before telemanipulation starts, we developed three alternative methods of determining the desired orientation for the manipulator effector, i.e. the real ultrasound probe:

- An incremental method that does not require synchronisation of any axis,

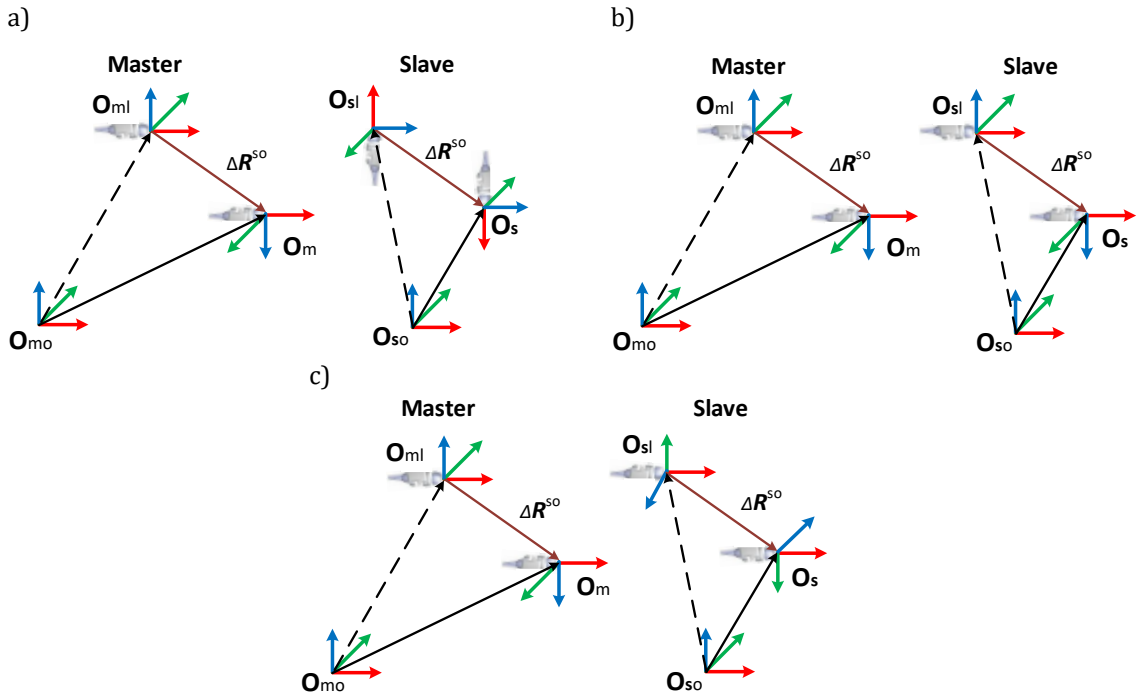

Fig. 11. Diagram showing the arrangement of the dummy and real probes at the moment of coupling and after rotation (with additional translation) of the input device by 180 degrees around the X (probe symmetry) axis
a – when no axis is synchronised at the time of system coupling - when synchronisation is not required, b – in the case of consistent arrangement of the dummy and real probes, c – when only the synchronisation of the X-axis is required

- A direct method that requires synchronisation of all axes,
- A mixed method requiring synchronisation only of the X axis (i.e. requiring a certain setting of the rotation angles of the axes Y and Z of the orientation input device.

In the case of the first proposed method (the incremental one) the desired orientation of the effector of the manipulator is directly calculated from the equations (13) and (14). Regardless of how the two probes are aligned at the time of the pedal coupling, the real probe will change its orientation by $\Delta \boldsymbol{R}^{so}$ (increment), relative to its initial orientation. Although from the point of view of proper operation of the control system, it does not require any specific settings of both probes relative to each other (synchronisation), in the case where the coupling occurs with both probes heavily misaligned, the pose handling becomes non-intuitive for the doctor. This problem is presented in Fig. 11a, where the probes at the time of coupling are rotated relative to each other by 180 degrees and the rotation of the input device (dummy probe) around its axis of symmetry, i.e. the X-axis causes a rotation of the real probe not around its axis of symmetry but around the perpendicular axis (i.e. the Z axis). To eliminate this, the coupling must be forced after both systems are synchronised in all axes, which is quite a troublesome and above all time-consuming operation for the doctor.

To implement the second method (the direct one) in the equation (13) instead of the rotation matrix representing the orientation of the input device at the time of coupling, one should use the orientation matrix for which the coordinate system of the input device assumes an initial orientation (i.e., the one for which all rotation angles are zero). Considering the fact that the matrix is the identity matrix, equation (13) is simplified to the form:

$$\Delta \boldsymbol{R}^{so} = \boldsymbol{R}_m^{so}. \tag{15}$$

A similar procedure should be taken with the equation (14), in which, instead of the rotation matrix representing the orientation of the effector of the manipulator at the moment of coupling, one should use the orientation matrix for which an actual coordinate system of the ultrasound probe assumes an orientation output $\boldsymbol{R}_s^{so}(0) \in \mathbb{R}^{3x3}$ (i.e. when all the angles of the manipulator are zero). Then the desired rotation matrix for the real ultrasound probe is determined as follows:

$$\boldsymbol{R}_d = \boldsymbol{R}_s^{so} = \boldsymbol{R}_m^{so} \boldsymbol{R}_s^{so}(0). \tag{16}$$

In this method, from the point of view of the intuitive handling by the doctor, a prior synchronisation would not be required. However, the coupling of the systems when the coordinate systems are not aligned with each other, generates a rapid, often dangerous movement of the real probe. Therefore, for safety reasons, it is required to introduce a requirement of prior synchronisation of all axes (see Fig. 11b).

The implementation of the third (mixed) method requires the modification of the second method. In the method of mixed orientation change caused by the input device in the axes Z and Y is carried out as in the second method, and the change in orientation caused by rotation about the X-axis (axis of symmetry of the

dummy probe) is realised by the incremental method. To achieve this, first the rotation matrix of the slave manipulator registered at the time of coupling is converted to the Euler angles representation, consistent with the representation of the rotation matrix of the input device expressed by equation (11). Due to the condition of having to synchronise the X-axis of the two probes (i.e. setting the rotation angles of the Y and Z axes of the input device so that: $\varphi_{sz} = \varphi_{mz}$ and $\varphi_{sy} = \varphi_{my}$), one should additionally compute an equivalent to the angle of rotation φ_{sxl} about the X axis. Finally, the desired rotation matrix for the real ultrasound probe is calculated according to:

$$\boldsymbol{R}_d = \boldsymbol{R}_s^{so} = \boldsymbol{R}_{z,\varphi sz}\boldsymbol{R}_{y,\varphi sy}\boldsymbol{R}_{x,\varphi sx}\boldsymbol{R}_s^{so}(0), \tag{17}$$

wherein the angle φ_{sx} by which the coordinate system of the manipulator should be rotated around the axis X, is:

$$\varphi_{sx} = \varphi_{sxl} + \varphi_{mxl} - \varphi_{mx}, \tag{18}$$

where: φ_{mx} and φ_{mxl} are the rotation angles of the input device about the X axis - respectively the current one and the one registered at the time of coupling of the master and slave.

The moment of synchronisation and change of the orientation of the implemented mixed method is shown by the diagram in Fig. 11c. It is evident there that at any point in time only the X-axes of the two probes are consistent with each other. This synchronisation ensures full intuitiveness of the operation of the orientation change by the doctor for the real probe, e.g. when it forces a pivoting movement of the probe during the examination. Then the alignment of the other two axes is not important for the doctor.

5. Summary

The system for control of the position and orientation of the manipulator, presented in this article, has been implemented in a real, functioning in the form of a prototype, ReMeDi system used to perform teleechography. The entire system was subjected to evaluation with the participation of specialists and patient volunteers. Evaluations have confirmed the correctness of the system and provided information on, among others, the choice of the solutions discussed in the section 4.2 i.e. the methods of determining the desired orientation. Although the incremental method, in order to work properly, does not require the troublesome synchronisation of the probes, yet it causes non-intuitive controls of the orientation, which are the greater the more the probes are out of sync. Therefore, the most useful is the mixed method, which requires only the alignment of the axis of symmetry of the two probes. It increase the comfort of the doctor's work and shortens the time of the examination performed.

AUTHORS

Adam Kurnicki* – Automation and Metrology Department, Faculty of Electrical Engineering and Computer Science, Lublin University of Technology, ul. Nadbystrzycka 38a, 20-618 Lublin, Poland, e-mail: a.kurnicki@pollub.pl, www.pollub.pl.

Bartłomiej Stańczyk – ACCREA Engineering, ul. Hiacyntowa 20, 20-143 Lublin, Poland, e-mail: b.stanczyk@accrea.com, www.accrea.com.

*Corresponding author

ACKNOWLEDGEMENTS

This work was supported by the European Commission FP7 ICT-610902 project ReMeDi (Remote Medical Diagnostician) and by Lubelska Agencja Wspierania Przedsiębiorczości within the "Research and innovation" activity 1.2 RPO WL 2014-2020.

REFERENCES

[1] "AdEchoTech – the manufacturer website". http://www.adechotech.com/products/. Accessed on: 12.08.2019.

[2] "Medirob – the manufacturer website". http://www.medirob.se. Accessed on: 12.08.2019.

[3] "Remote Medical Diagnostician | ReMeDi Project | FP7 | CORDIS | European Commission". https://cordis.europa.eu/project/rcn/110646/factsheet/en. Accessed on: 28.08.2019.

[4] "VGo – the manufacturer website". http://www.vgocom.com/. Accessed on: 12.08.2019.

[5] P. Arbeille, J. Ayoub, V. Kieffer, P. Ruiz, B. Combes, A. Coitrieux, P. Herve, S. Garnier, B. Leportz, E. Lefbvre, and F. Perrotin, "Realtime Tele-Operated Abdominal and Fetal Echography in 4 Medical Centres, from one Expert Center, using a Robotic Arm & ISDN or Satellite Link". In: *2008 IEEE International Conference on Automation, Quality and Testing, Robotics*, vol. 1, 2008, 45–46, 10.1109/AQTR.2008.4588703.

[6] K. Arent, M. Cholewiński, Ł. Chojnacki, W. Domski, M. Drwięga, J. Jakubiak, M. Janiak, B. Kreczmer, A. Kurnicki, B. Stańczyk, and D. Szczęśniak-Stańczyk, "Selected Topics in Design and Application of a Robot for Remote Medical Examination with the Use of Ultrasonography and Ascultation from the Perspective of the REMEDI Project", *Journal of Automation, Mobile Robotics and Intelligent Systems*, vol. 11, no. 2, 2017, 82–94, 10.14313/JAMRIS_2-2017/20.

[7] S. Avgousti, A. S. Panayides, E. G. Christoforou, A. Argyrou, A. Jossif, P. Masouras, C. Novales, and P. Vieyres, "Medical Telerobotics and the Remote Ultrasonography Paradigm Over 4G Wireless Networks". In: *2018 IEEE 20th International Conference on e-Health Networking, Applications and Services (Healthcom)*, 2018, 1–6, 10.1109/HealthCom.2018.8531194.

[8] C. A. Avizzano, A. Filippeschi, J. M. J. Villegas, and E. Ruffaldi, "An Optimal Geometric Model

for Clavels Delta Robot". In: *2015 IEEE European Modelling Symposium (EMS)*, 2015, 232–237, 10.1109/EMS.2015.84.

[9] F. Courreges, P. Vieyres, and R. S. H. Istepanian, "Advances in robotic tele-echography services - the OtelO system". In: *The 26th Annual International Conference of the IEEE Engineering in Medicine and Biology Society*, vol. 2, 2004, 5371–5374, 10.1109/IEMBS.2004.1404499.

[10] S. S. Gadupudi, S. Nisha, and S. Yarramasu, "Teledentistry: A futuristic realm of dental care", *International Journal of Oral Health Sciences*, vol. 7, no. 2, 2017, 63–67, 10.4103/ijohs.ijohs_22_17.

[11] N. Koizumi, S. Warisawa, H. Hashizume, and M. Mitsuishi, "Continuous Path Controller for the Remote Ultrasound Diagnostic System", *IEEE/ASME Transactions on Mechatronics*, vol. 13, no. 2, 2008, 206–218, 10.1109/TMECH.2008.918530.

[12] N. Koizumi, S. Warisawa, M. Nagoshi, H. Hashizume, and M. Mitsuishi, "Construction Methodology for a Remote Ultrasound Diagnostic System", *IEEE Transactions on Robotics*, vol. 25, no. 3, 2009, 522–538, 10.1109/TRO.2009.2019785.

[13] A. Krupa, D. Folio, C. Novales, P. Vieyres, and T. Li, "Robotized Tele-Echography: An Assisting Visibility Tool to Support Expert Diagnostic", *IEEE Systems Journal*, vol. 10, no. 3, 2016, 974–983, 10.1109/JSYST.2014.2314773.

[14] A. Kurnicki, M. Cholewiński, B. Stańczyk, and K. Arent, "Implementation and evaluation of a bilateral teleoperation with use of wave variables in the ReMeDi system for remote medical examination". In: *2017 22nd International Conference on Methods and Models in Automation and Robotics (MMAR)*, 2017, 131–136, 10.1109/MMAR.2017.8046811.

[15] A. Kurnicki, B. Stańczyk, and B. Kania, "Manipulator Development for Telediagnostics". In: *Proceedings of the International Conference on Mechatronics and Robotics, Structural Analysis (MEROSTA2014)*, 2014, 214–218.

[16] K. Mathiassen, J. E. Fjellin, K. Glette, P. K. Hol, and O. J. Elle, "An Ultrasound Robotic System Using the Commercial Robot UR5", *Frontiers in Robotics and AI*, vol. 3, 2016, 10.3389/frobt.2016.00001.

[17] R. Monfaredi, E. Wilson, B. Azizi Koutenaei, B. Labrecque, K. Leroy, J. Goldie, E. Louis, D. Swerdlow, and K. Cleary, "Robot-assisted ultrasound imaging: Overview and development of a parallel telerobotic system", *Minimally invasive therapy & allied technologies: MITAT: official journal of the Society for Minimally Invasive Therapy*, vol. 24, no. 1, 2015, 54–62, 10.3109/13645706.2014.992908.

[18] A. S. B. Mustafa, T. Ishii, Y. Matsunaga, R. Nakadate, H. Ishii, K. Ogawa, A. Saito, M. Sugawara, K. Niki, and A. Takanishi, "Development of robotic system for autonomous liver screening using ultrasound scanning device". In: *2013 IEEE International Conference on Robotics and Biomimetics (ROBIO)*, 2013, 804–809, 10.1109/ROBIO.2013.6739561.

[19] A. Niewola, L. Podsędkowski, P. Wróblewski, P. Zawiasa, and M. Zawierucha, "Selected aspects of robin heart robot control", *Archive of Mechanical Engineering*, vol. LX, no. 4, 2013.

[20] C. Passenberg, A. Peer, and M. Buss, "A survey of environment-, operator-, and task-adapted controllers for teleoperation systems", *Mechatronics*, vol. 20, no. 7, 2010, 787–801, 10.1016/j.mechatronics.2010.04.005.

[21] A. Peer, M. Buss, B. Stanczyk, D. Szczesniak-Stanczyk, W. Brzozowski, A. Wysokinski, M. Tscheligi, C. A. Avizzano, E. Ruffaldi, L. van Gool, A. Fossati, K. Arent, J. Jakubiak, and M. Janiak, "Towards a remote medical diagnostician for medical examination". In: *NextMed MMVR21*, 2014.

[22] A. Peretti, F. Amenta, S. K. Tayebati, G. Nittari, and S. S. Mahdi, "Telerehabilitation: Review of the State-of-the-Art and Areas of Application", *JMIR Rehabilitation and Assistive Technologies*, vol. 4, no. 2, 2017, 10.2196/rehab.7511.

[23] L. Santos and R. Cortesão, "Admittance control for robotic-assisted tele-echography". In: *2013 16th International Conference on Advanced Robotics (ICAR)*, 2013, 1–7, 10.1109/ICAR.2013.6766502.

[24] L. Santos and R. Cortesão, "Computed-Torque Control for Robotic-Assisted Tele-Echography Based on Perceived Stiffness Estimation", *IEEE Transactions on Automation Science and Engineering*, vol. 15, no. 3, 2018, 1337–1354, 10.1109/TASE.2018.2790900.

[25] B. Stańczyk, A. Kurnicki, and K. Arent, "Logical architecture of medical telediagnostic robotic system". In: *2016 21st International Conference on Methods and Models in Automation and Robotics (MMAR)*, 2016, 200–205, 10.1109/MMAR.2016.7575133.

[26] B. Stanczyk, A. Peer, and M. Buss, "Development of a high-performance haptic telemanipulation system with dissimilar kinematics", *Advanced Robotics*, vol. 20, no. 11, 2006, 1303–1320, 10.1163/156855306778792461.

[27] G. Stollnberger, C. Moser, C. Zenz, M. Tscheligi, D. Szczesniak-Stanczyk, M. Janowski, W. Brzozowski, and A. Wysokinski, "Capturing expected user experience of robotic systems in the health care sector". In: *Proceedings of the Austrian Robotics Workshop 2014*, 2014, 42–46.

[28] Á. Takács, S. Jordán, D. Á. Nagy, J. K. Tar, I. J. Rudas, and T. Haidegger, "Surgical robotics — Born in space". In: *2015 IEEE 10th Jubilee International Symposium on Applied Computational Intelligence and Informatics*, 2015, 547–551, 10.1109/SACI.2015.7208264.

[29] J. M. J. Villegas, C. A. Avizzano, E. Ruffaldi, and M. Bergamasco, "A Low Cost Open-Controller for Interactive Robotic System". In: *2015 IEEE European Modelling Symposium (EMS)*, 2015, 462–468, 10.1109/EMS.2015.75.

[30] J. Zhou, X. Ma, Z. Xu, and Z. Qi, "Overview of Medical Robot Technology Development". In: *2018 37th Chinese Control Conference (CCC)*, 2018, 5169–5174, 10.23919/ChiCC.2018.8483769.

[31] W. Zhu, S. E. Salcudean, S. Bachmann, and P. Abolmaesumi, "Motion/force/image control of a diagnostic ultrasound robot". In: *Proceedings 2000 ICRA. Millennium Conference. IEEE International Conference on Robotics and Automation*, vol. 2, 2000, 1580–1585, 10.1109/ROBOT.2000.844822.